Jurnal Ilmiah Matematika dan Pendidikan Matematika (JMP)
Vol. 17 No. 2, Desember 2025, hal. 115-132
ISSN (Cetak) : 2085-1456; ISSN (*Online*) : 2550-0422

ASYMPTOTIC STUDY OF NONLINEAR SPRING OSCILLATION WITH EXTERNAL FORCE USING THE MULTIPLE TIME SCALES METHOD

Glagah Eskacakra Setyowisnu*

Universitas Jenderal Soedirman
glagah.setyowisnu@unsoed.ac.id

Lilik Muzdalifah

Universitas Jenderal Soedirman
lilik.muzdalifah@unsoed.ac.id

Isnu Aji Saputro

Universitas Jenderal Soedirman
isnu.saputro@unsoed.ac.id

ABSTRACT. *A nonlinear spring is a type of oscillator that does not follow Hooke's law perfectly. In mathematics, this type of oscillator can be modeled in a nonlinear ordinary differential equation. Of the many discussions on oscillation models, one examines the behavior of the model when disturbed by a parameter with a very small value. In this study, a discussion will be conducted regarding the behavior of the oscillation model with external forces added to the disturbance parameters in the damping and spring stiffness terms. To observe this behavior, one of the techniques in asymptotic analysis called the multiple time scales method is used. The results of this study will show the behavior of the oscillation model with the disturbance parameters caused by the resonance that occurs. To provide a clearer picture, the oscillations that occur are presented in the form of a simulation result graph, containing a comparison between the approximate solution and the numerical solution. Based on the discussion given, it is concluded that the oscillations in the model are strongly influenced by a certain relationship between the natural frequency of the nonlinear spring and the frequency of the external force acting on the model.*

Keywords*: asymptotic analysis, multiple time scales, oscillation model, nonlinear spring, resonance.*

ABSTRAK. Suatu pegas tak linier merupakan salah satu jenis osilator yang tidak mengikuti hukum Hooke secara sempurna. Dalam matematika, osilator jenis ini dapat dimodelkan dalam suatu persamaan diferensial biasa tak linier. Dari banyak diskusi yang membahas model osilasi, salah satunya mengkaji perilaku dari model ketika diganggu oleh suatu parameter yang bernilai sangat kecil. Pada penelitian ini akan dilakukan pembahasan mengenai perilaku dari model osilasi dengan gaya luar yang ditambahkan parameter gangguan pada suku redaman dan kekakuan pegas. Untuk melihat perilaku tersebut, digunakan salah satu teknik dalam analisis asimtotik yang disebut metode multiple time scales. Hasil dari penelitian ini akan menunjukkan perilaku dari model osilasi dengan parameter gangguan yang diakibatkan oleh resonansi yang terjadi. Guna

*Corresponding Author
Article Info: submitted 18 October 2025; revised 18 December 2025; accepted 31 December 2025.

memberikan gambaran yang lebih jelas, osilasi yang terjadi disajikan dalam bentuk grafik hasil simulasi, memuat perbandingan antara solusi hampiran dan solusi numerik. Berdasarkan pembahasan yang diberikan, disimpulkan bahwa osilasi pada model sangat dipengaruhi oleh hubungan tertentu antara frekuensi alami pegas tak linier dengan frekuensi gaya luar yang bekerja pada model.

Kata Kunci: Analisis asimtotik, multiple time scales, model osilasi, pegas tak linier, resonansi.

1. INTRODUCTION

The integration of human social life with technology has brought the world into the era of society 5.0. The existence of technology today helps make modern human life easier, and has resulted in an increase in human needs for materials to support this technology (Kariarta, 2020). Of the many types of technology, some require oscillators with damping so that the system can work properly and reduce risks in its use. In physics, an oscillator is a periodic motion system that passes through an equilibrium point for a certain period of time (Kusumadjati, et al., 2017). The oscillator itself is one of the important things in engineering that continues to be studied in depth. One type of oscillator is a spring, which is often associated with Hooke's law. It does not apply perfectly to nonlinear springs, because the approximation to Hooke's law is linear. Due to its nonlinearity, nonlinear spring models cannot be solved explicitly. In mathematics, these models are given as nonlinear ordinary differential equations.

Several studies that discuss nonlinear spring models are often associated with the Duffing equation. For example, research conducted by Illahi et al. (2024) investigated the solution of the Duffing equation using exponential time differencing method and showed its effectiveness for strongly nonlinear differential equations. There is also Guang-Qing Feng (2021) who discussed the approximate frequency of a fractal oscillator in the undamped duffing equation, using the two-scale transform method and the fractal frequency formula. In addition, there is research conducted by Tarini K. Dutta and Pramila K. Prajapati (2016) which discussed the dynamic properties of the nonlinear duffing equation with damping terms and external forces. The study showed that the model behaves in a periodic and chaotic behavior even though it is given a perturbation

in the form of a linear term.

Another research on the Duffing equation has also been conducted by Gusrian Putra et al. (2023) who discussed the solution of the homogeneous Duffing oscillator equation using the multiple scales method, which is included in the asymptotic solution method. In the same study, Gusrian Putra et al. (2023) showed the existence of limit cycles in the dynamics of the duffing equation used. The same method was also used by Eric Harjanto et al. (2021) in studying the resonance of a weak nonlinear microbeam caused by electric actuation in two parts. The first part of the paper provides accurate approximations of the natural frequencies as well as the superharmonic and subharmonic resonance frequencies of the actuated microbeam up to order ε^3, while the second part considers a viscous damping term of order ε and structural damping and nonlinar elastic forces of order ε^2.

Furthermore, another study that apply the multiple time scale method has also been carried out on a certain model, such as that carried out by Nikenasih et al. (2024) who presented a new approach to applying this method to delay differential equations. The paper shows that the infinitely many roots of the characteristic equation of the delay differential equations can be taken into account, and the initial condition over the time interval determined by the delay can be satisfied. Besides that,

In this study, the equation studied is included in the nonhomogeneous and nonlinear ordinary differential equations. Using the multiple time scales method, we will discuss the asymptotic analysis of the nonlinear oscillation equation, where the equation is given a very small perturbation on the damping term and the nonlinear term. In contrast to Tarini K. Dutta and Pramila K. Prajapati (2016) which only considered the dynamical behavior of the forced spring equation, the study in this research focuses on the behavior of springs resulting from the relationship between the natural frequency and the frequency of the excitation force. This study also investigates superharmonic and subharmonic resonance, similar to the work conducted by Eric Harjanto et al. (2021). However, the analysis is limited to the order of ε, with a relatively brief discussion that is

nonetheless sufficient to provide an overview of the model's behavior. Furthermore, the simulation will present a comparison between two curves, each of which is generated by the asymptotic solution and also the numerical solution resulting from the Runge-Kutta method available in Python software. The differences between the two simulations performed will also be visualized in the absolute error graph. Thus, this study contributes to a clearer understanding of the effects of resonance on the behavior of nonlinear springs under small perturbations.

2. METHODS

This research was conducted by reviewing the literature on previous studies. Several things related to the methods used will be discussed in this section. Multiple time scales method is used as an asymptotic analytical method, while the Dormand-Prince scheme – a family of Runge-Kutta methods – is used directly using a function in Python software as a numerical approach. Furthermore, the data used is simulated data intended solely for visualization, where the visualization will demonstrate the behavior of the mathematical model being studied.

2.1 Multiple-Scales Expansions

In oscillatory problems with small perturbation, the solution oscillates on the time scale $\mathcal{O}(1)$ and experiences slow variations on the time scale $\mathcal{O}\left(\frac{1}{\varepsilon}\right)$, so that the variables $t_0 = t$ and $t_1 = \varepsilon^{\alpha} t$ are introduced to accommodate both time scales. These two time scales will be treated as independent regarding to Mark H. Holmes (2013), resulting in a consequence on the original time derivative transforming as follows

$$\frac{d}{dt} \rightarrow \frac{dt_0}{dt}\frac{\partial}{\partial t_0} + \frac{dt_1}{dt}\frac{\partial}{\partial t_1} = \frac{\partial}{\partial t_0} + \varepsilon^{\alpha}\frac{\partial}{\partial t_1}. \tag{1}$$

To simplify the notation, we will use the symbols D_0 and D_1 in place $\frac{\partial}{\partial t_0}$ and $\frac{\partial}{\partial t_1}$, respectively.

2.2 Runge-Kutta Methods

This method attains accuracy comparable to the Taylor series approach while avoiding the need to compute higher-order derivatives. Regarding to Chapra and Canale (2015), the generalized form of the formula of this method is

$$x_{i+1} = x_i + \phi(t_i, x_i, h)h \tag{2}$$

where x_i, x_{i+1}, and h are the new value, old value, and distance, respectively. The function of $\phi(t_i, x_i, h)$ is called the increment function, which can be interpreted as a representative slope over the interval, and can be written in the general form as

$$\phi = c_1k_1 + c_2k_2 + \cdots + c_nk_n \tag{2}$$

where the c's are constants and the k's are

$$k_1 = f(t_i, x_i) \tag{3a}$$

$$k_2 = f(t_i + p_1h, x_i + q_{11}k_1h) \tag{3b}$$

$$k_3 = f(t_i + p_2h, x_i + q_{21}k_1h + q_{22}k_2h) \tag{3c}$$

$$\vdots$$

$$k_n = f\left(t_i + p_{n-1}h, x_i + \sum_{j=1}^{n-1} q_{(n-1)j}k_jh\right) \tag{3d}$$

where the p's and the q' are constants.

The higher the order of the Runge-Kutta, the higher the accuracy. We use the algorithm of "RK45" in Python, which implements the Dormand-Prince scheme. This is a Runge-Kutta method that uses both 4th and 5th order approximations.

3. RESULTS AND DISCUSSIONS

Let the oscillation model with an external force $F(t)$ given by

$$\ddot{u} + \omega^2u = \varepsilon(-\mu\dot{u} - ku\dot{u}) + F(t), \mu > 0, k \neq 0, 0 < \varepsilon \ll 1 \tag{4}$$

where $u = u(t)$ denotes the spring's position at time t. Furthermore ω, μ, and k are the natural frequency, damping parameter, and the stiffness of the spring, respectively. Suppose $F(t) = A\cos\Omega t = \frac{A}{2}e^{i\Omega t} + c.c.$ is an external force with frequency Ω and amplitude A, where $c.c.$ is the complex conjugate term. In this study, we will analyze the primary resonance scenario $(\Omega \approx \omega)$ and the secondary

resonance case ($\Omega \neq \omega$). Both scenarios will only be discussed up to the $\mathcal{O}(\varepsilon)$ because it is sufficient to approach an analytical solution and to simplify the discussion.

3.1 Primary Resonance Scenario ($\boldsymbol{\Omega \approx \omega}$)

Given a detuning parameter $\sigma = \mathcal{O}(1)$ which is written as $\Omega = \omega + \varepsilon\sigma$. Suppose the excitation amplitude $A = \mathcal{O}(\varepsilon)$ as $A = \varepsilon a$ and $a = \mathcal{O}(1)$. By applying multiple two-time scales, we can write $u(t,\varepsilon) = u_0(T_0, T_1) + \varepsilon u_1(T_0, T_1) + \cdots$ with $T_n = \varepsilon^n t$, while $\frac{d}{dt} = D_0 + \varepsilon D_1$ and $\frac{d^2}{dt^2} = D_0^2 + 2\varepsilon D_0 D_1 + \varepsilon^2 D_1^2$ are the differential operators for multiple two-time scales. By applying both differential operators toward $u(t)$ in Equation (4), we will have two ODEs as follows.

$$\mathcal{O}(1): D_0^2 u_0 + \omega^2 u_0 = 0 \tag{5}$$

$$\mathcal{O}(\varepsilon): D_0^2 u_1 + \omega^2 u_1 = D_0(\mu - 2D_1 - \alpha u_0)u_0 + \frac{a}{2} e^{i(T_0\omega + T_1\sigma)} + c.c. \tag{6}$$

We can see that $\mathcal{O}(1)$-problem is a homogeneous linear ODE which has solution as follows,

$$u_0(T_0, T_1) = C(T_1)e^{i\omega T_0} + \bar{C}(T_1)e^{-i\omega T_0} \tag{7}$$

By substituting Solution (7) into $\mathcal{O}(\varepsilon)$-problem in Equation (6), we will have a nonhomogeneous linear ODE that can be seen below.

$$D_0^2 u_1 + \omega^2 u_1 = -i\omega k C^2 e^{2i\omega T_0} + \left(\frac{a}{2} e^{iT_1\sigma} - i\omega(2D_1 C + \mu C\right) e^{i\omega T_0} + c.c. \tag{8}$$

As we can see that a secular term is present in Equation (8) and it should be neglected for the solvability condition. Let $C(T_1) = \frac{1}{2} c e^{ib}$ where c and b are variables with respect to T_1. Then, we will have an equation with real and imaginary parts. If both parts are zeroed, we will have

$$Re: cb' = -\frac{a}{2\omega}\cos(\sigma T_1 - b) \tag{9}$$

$$Im: c' = \frac{a}{2\omega}\sin(\sigma T_1 - b) - \frac{\mu}{2} c \tag{10}$$

Now, denote $\gamma = \sigma T_1 - b$ so that $\gamma' = \sigma - b'$, thus Equation (9) and (10) can be written as Equation (11) and (12), respectively, whereas an autonomous system.

$$Re: c\gamma' = \frac{a}{2\omega}\cos(\gamma) + c\sigma \tag{11}$$

$$Im: c' = \frac{a}{2\omega}\sin(\gamma) - \frac{\mu}{2}c \tag{12}$$

Furthermore, steady state solution can be obtained while $c' = \gamma' = 0$ while (c_s, γ_s) is a singular point that satisfies Equation (13) and (14).

$$\sigma c_s = -\frac{a}{2\omega}\cos(\gamma_s) \tag{13}$$

$$\frac{\mu}{2}c_s = \frac{a}{2\omega}\sin(\gamma_s) \tag{14}$$

From those two equations above, we will have a frequency of response equation. Hence, we can obtain a function of detuning parameter σ as

$$\sigma = \pm\frac{1}{2}\sqrt{\left(\frac{a}{c_s\omega}\right)^2 - \mu^2}. \tag{15}$$

Now, the steady state solution where $C(T_1) = \frac{1}{2}c_s e^{ib_s}$, $c_s \notin \mathbb{C}$, and $b_s = \sigma T_1 - \gamma_s$ can be seen in Solution (16).

$$u_s \approx c_s \cos(\Omega t - \gamma_s) + \mathcal{O}(\varepsilon) \tag{16}$$

The simulation of this scenario is presented in Figure 1 that shows both asymptotic and numerical solution. Figure 1a shows a fairly rapid decrease in amplitude at $t \in [0,50]$. In addition, the behavior of the nonlinear spring also does not show periodic motion at this time interval. It can be seen that the movement of the spring is quite chaotic.

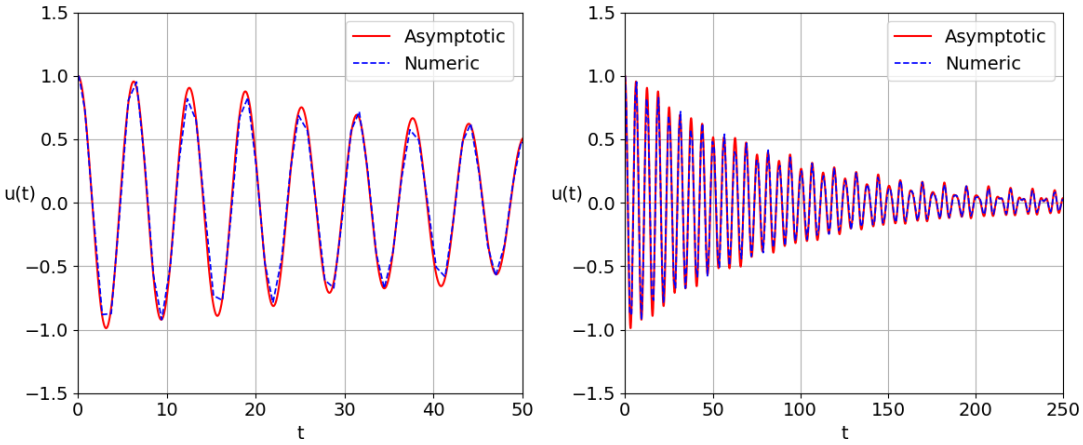

a. $t \in [0,50]$ b. $t \in [0,250]$

Figure 1. Visualization of primary resonance scenario with $a = 1$, $\mu = 0.5$, $\omega = 1$, $\sigma = 10$, $\Omega = \omega + \varepsilon\sigma$, $k = 1$, and $\varepsilon = 0.05$.

It can also be seen in Figure 1b for further interval, that the oscillations of the nonlinear spring have a smaller amplitude. The figure shows that there is a slight

increase in amplitude caused by the primary resonance effect for $t > 50$. After reaching a certain time, the spring will only move around the equilibrium point for a very long time because the form of the solution is a periodic function, and does not converge to the equilibrium point. Furthermore, the differences between the two methods are available in Figure 2, where the absolute error value becomes relatively small for longer times.

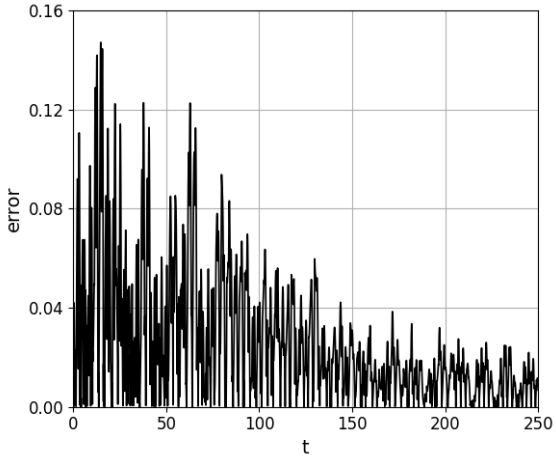

Figure 2. Absolute error of asymptotic and numerical solution for primary resonance scenario

3.2 Secondary Resonance Scenario ($\boldsymbol{\Omega \neq \omega}$)

In this scenario, the amplitude $A = \mathcal{O}(1)$ so that the external force dan be written as $F(t) = \frac{A}{2}e^{i\Omega t} + c.c.$. By using the same procedure as the primary resonance scenario, we will have

$$\mathcal{O}(1): D_0^2 u_0 + \omega^2 u_0 = \frac{A}{2}e^{i\Omega T_0} + c.c \tag{17}$$

$$\mathcal{O}(\varepsilon): D_0^2 u_1 + \omega^2 u_1 = [(\mu - \alpha u_0) - 2D_1]D_0 u_0. \tag{18}$$

We can see that Equation (17) can be solved directly by using the variation of parameters' method that presented as

$$u_0(T_0, T_1) = C(T_1)e^{i\omega T_0} + \Lambda e^{i\Omega T_0} + c.c. \tag{19}$$

where $\Lambda = \frac{A}{2(\omega^2 - \Omega^2)}$. Now, we consider Equation (18) substituted by $u_0(T_0, T_1)$ in Solution (19) in the form

$$D_0^2 u_1 + \omega^2 u_1 = \delta_1 e^{i\omega T_0} + \delta_2 e^{i\Omega T_0} + \delta_3 e^{2i\omega T_0} + \delta_4 e^{2i\Omega T_0} + \delta_5 e^{i(\Omega+\omega)T_0} + \delta_6 e^{i(\Omega-\omega)T_0} + \delta_7 e^{i(\omega-\Omega)T_0} + c.c. \tag{20}$$

where $\delta_1 = -i\omega(2D_1 + \mu)C$, $\delta_2 = -i\Omega\mu\Lambda$, $\delta_3 = -i\alpha\omega C^2$, $\delta_4 = -i\alpha\Omega\Lambda^2$, $\delta_5 = -i\alpha\bar{C}\Lambda(\Omega + \omega)$, $\delta_6 = -i\alpha\bar{C}\Lambda(\Omega - \omega)$, and $\delta_7 = -i\alpha C\Lambda(\omega - \Omega)$. It can be seen in Equation (20) that the secular term can be obtained from each term in the equation. Hence, the solvability conditions are devided in several cases such as superharmonic resonance, subharmonic resonance, and nonresonant. Superharmonic and subharmonic resonance states occur when $2\Omega \approx \omega$ and $\Omega \approx 2\omega$ respectively, while nonresonant state are when Ω is far enough from zero, $\frac{\omega}{2}$, or 2ω. In addition, we will also discuss a state when $\Omega \approx 0$. Furthermore, the $C(T_1)$ function will be denoted by $C(T_1) = \frac{1}{2}ce^{ib}$ as in the first scenario.

3.2.1 Nonresonant Case

For this case, the solvability condition gives $\delta_1 = 0$ so that we will have the real and imaginary parts zeroed out into the following two equations.

$$Re: cb' = 0 \tag{21}$$

$$Im: c' = -\frac{1}{2}\mu c \Leftrightarrow c = c_0 e^{-\frac{1}{2}\mu T_1} \tag{22}$$

Because $u = u_0 + \varepsilon u_1 + \cdots$, we will obtain the solution by substituting Equation (19) into $u(T_0, T_1)$. Thus, the solution for this case is as follows.

$$u = c\cos(\omega t + b) + \frac{A}{\omega^2 - \Omega^2}\cos(\Omega t) + \mathcal{O}(\varepsilon) \tag{23}$$

The visualization for nonresonant state is presented in the figure below.

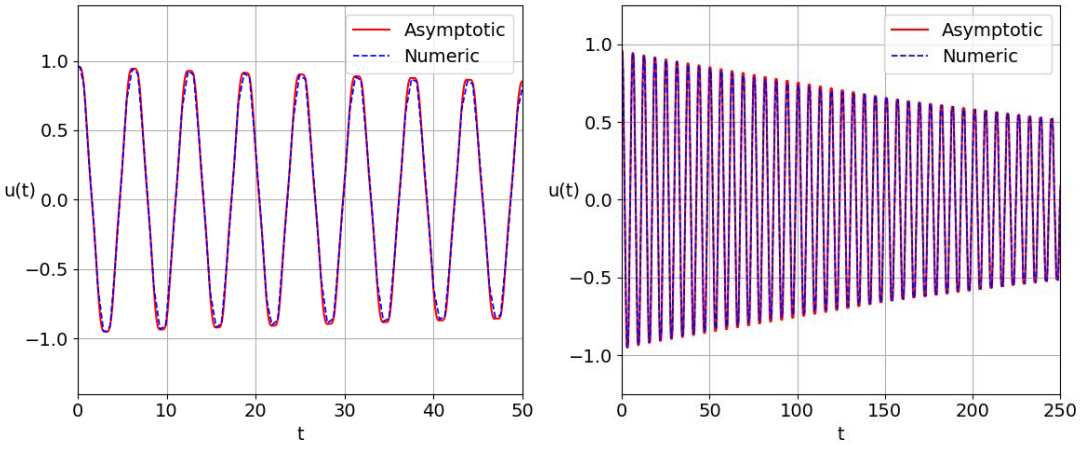

a. $t \in [0,50]$ b. $t \in [0,250]$

Figure 3. Visualization of nonresonant case with $A = 1$, $\mu = 0.5$, $\omega = 1$, $\sigma = 10$, $\Omega = 5$, $k = 1$, and $\varepsilon = 0.05$.

Figure 3 corresponds to the physical behavior of a spring that does not experience resonance in its oscillations, where the decrease in amplitude of the spring is relatively smooth and consistent. This kind of behavior continues for a longer time, as presented in Figure 3b. The parameters that work in this state are only the damping parameters and the spring stiffness. This is a basic comparison for the resonance behavior that occurs, which is called the free oscillation. Furthermore, the absolute error value for this scenario can be seen in Figure 4, where the value is also relatively small.

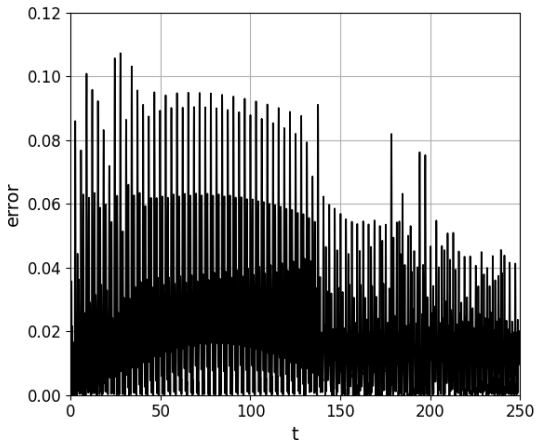

Figure 4. Absolute error of asymptotic and numerical solution for nonresonant scenario

3.2.2 Superharmonic Resonance Case

Let the detuning parameter being written in a formula $2\Omega = \omega + \varepsilon\sigma$. The solvability condition gives $\delta_1 + \delta_4 = 0$ so that by the same analogy as the nonresonant state and by denoting $\gamma = \sigma T_1 - b$, we will have the real and imaginary parts zeroed out into the following two equations.

$$c\gamma' = \frac{\alpha\Omega\Lambda^2}{\omega}\sin(\gamma) + \sigma c \tag{24}$$

$$c' = -\frac{\alpha\Omega\Lambda^2}{\omega}\cos(\gamma) - \frac{1}{2}\mu c \tag{25}$$

Since $2\Omega = \omega + \varepsilon\sigma$ and $u = u_0 + \varepsilon u_1 + \cdots$, we will obtain

$$u = c\cos(2\Omega t - \gamma) + \frac{A}{\omega^2 - \Omega^2}\cos(\Omega t) + \mathcal{O}(\varepsilon) \tag{26}$$

The visualization for superharmonic resonant state is presented in Figure 5. Superharmonic resonance has a significant impact on the oscillatory behavior of

nonlinear springs, because the natural frequency is greater than the excitation one. It can be seen in Figure 5a that the resulting amplitude is greater than the initial amplitude given. In addition, the resulting oscillatory motion is also not smooth, even more significantly than in the primary resonance scenario. This is because the energy from external forces is more efficiently absorbed by the system, so the system is at risk of instability when applied to real structures.

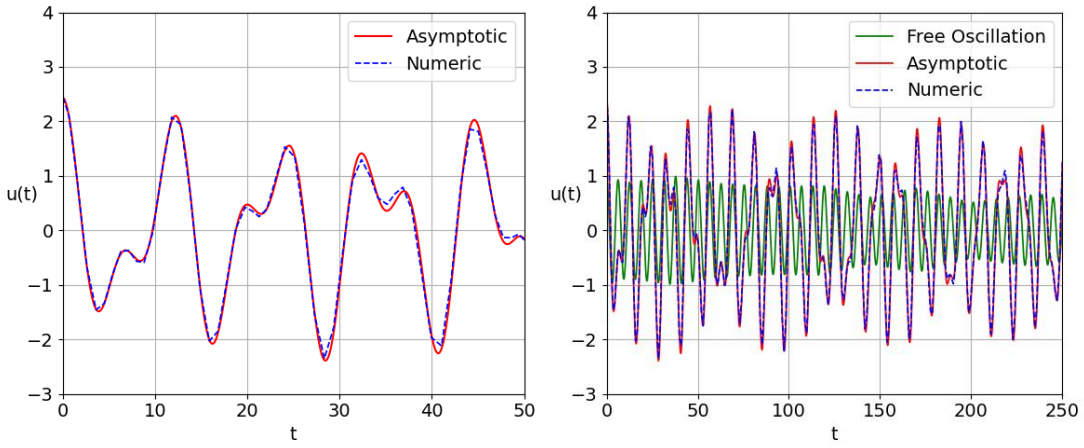

a. $t \in [0,50]$ b. $t \in [0,250]$

Figure 5. Visualization of superharmonic case with $A = 1$, $\mu = 0.5$, $\omega = 1$, $\sigma = 10$, $\Omega = \frac{\omega+\varepsilon\sigma}{2}$, $k = 1$, and $\varepsilon = 0.01$.

Further, the amplitude of the oscillation of the spring is decreasing very slowly as time goes by, as presented in Figure 5b. It can be seen in Figure 5b that the amplitude due to superharmonic resonance is much larger than the free oscillation curve. We can see a chaotic behavior. We can also see the chaotic behavior throughout the time interval clearly. In addition, the absolute error value for superharmonic resonance scenario can be seen in Figure 6, where the value is fluctuating and relatively small.

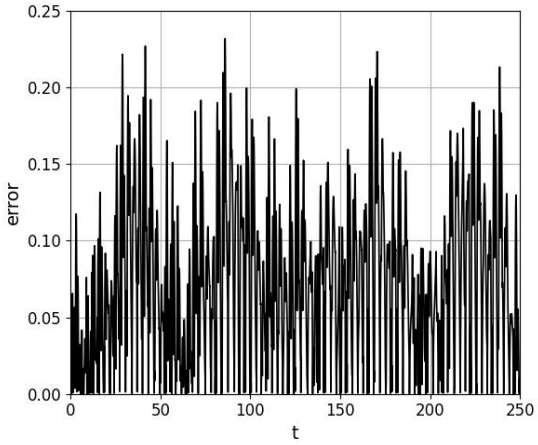

Figure 6. Absolute error of asymptotic and numerical solution for superharmonic resonance scenario.

3.2.3 Subharmonic Resonance Case

In this case, the detuning parameter being written in a formula $\Omega = 2\omega + \varepsilon\sigma$. The solvability condition gives $\delta_1 + \delta_6 = 0$ so that by the same analogy as before, we will also have the real and imaginary parts zeroed out into the following two equations.

$$Re: \gamma' = \sigma + \frac{\alpha\Lambda}{\omega}(\Omega - \omega)\sin(\gamma) \tag{27}$$

$$Im: c' = -\frac{1}{2}\mu c - c\frac{\alpha\Lambda}{\omega}(\Omega - \omega)\cos(\gamma) \tag{28}$$

Because of $\Omega = 2\omega + \varepsilon\sigma$ and $u = u_0 + \varepsilon u_1 + \cdots$, we will obtain

$$u = c\cos\left(\frac{1}{2}(\Omega t - \gamma)\right) + \frac{A}{\omega^2 - \Omega^2}\cos(\Omega t) + \mathcal{O}(\varepsilon) \tag{29}$$

The visualization for subharmonic resonant state is presented in Figure 7. We can not tell much when we look at Figure 7a, which visualizes the solution of a nonlinear spring under the influence of subharmonic resonance in the time interval $t \in [0,50]$, because we do not yet see any specific behavior there. However, things will be different if we look at Figure 7b, which has longer time interval.

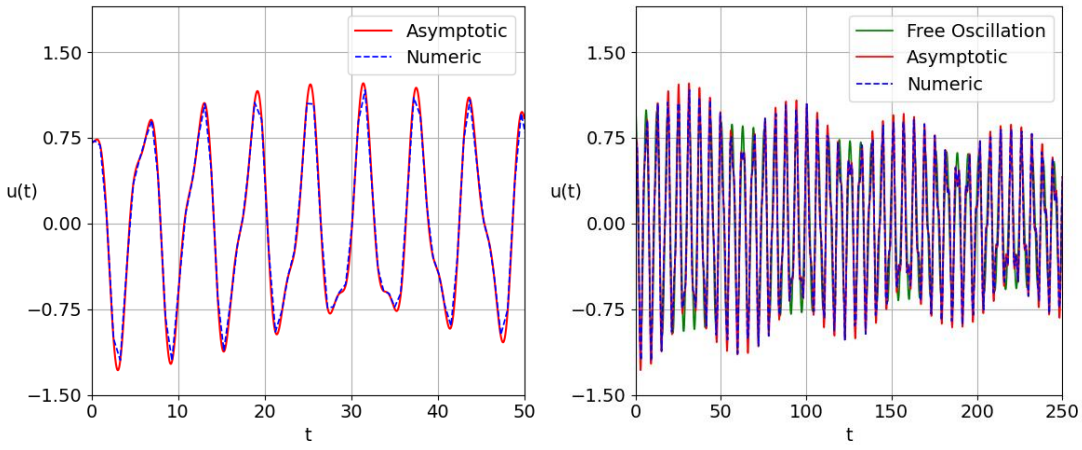

a. $t \in [0,50]$ b. $t \in [0,250]$

Figure 7. Visualization of subharmonic case with $A = 1$, $\mu = 0.5$, $\omega = 1$, $\sigma = 10$, $\Omega = 2\omega + \varepsilon\sigma$, $k = 1$, and $\varepsilon = 0.01$.

We know that the natural frequency is smaller than the excitation one, thus the oscillation can be forced. Eventhough the resulting amplitude is greater than the initial amplitude given, the oscillatory motion is relatively smooth as shown in Figure 7b. It shows that the nature of forced oscillation is still relatively controlled. Furthermore, we can see that the amplitude of the oscillation of the spring is also decreasing slowly in a certain pattern as the time goes by. In addition, the absolute error value for subharmonic resonance scenario can be seen in Figure 8, where the value is still fluctuating and relatively small.

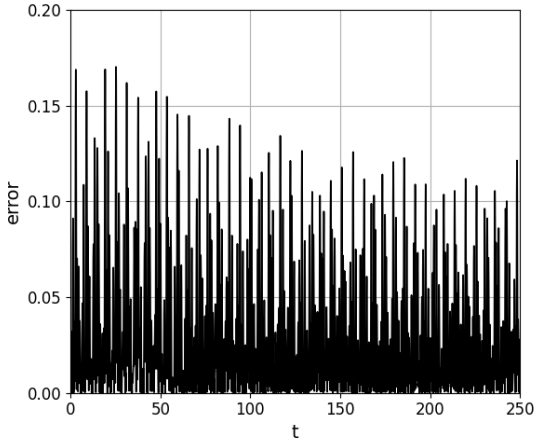

Figure 8. Absolute error of asymptotic and numerical solution for subharmonic resonance scenario.

3.2.4 A Certain Case Where $\Omega \approx 0$

In this final case, the frequency of the external force is close to zero so that the detuning parameter being written in a formula $\Omega = \varepsilon\sigma$. The solvability condition gives $\delta_1 + \delta_5 + \delta_7 = 0$ so that by the same analogy as before, we will have the b and c from the real and imaginary parts zeroed out into the following two equations.

$$Re: b = \frac{\Omega\alpha\Lambda}{\omega\sigma}\cos(\sigma T_1) \tag{30}$$

$$Im: c = c_0 e^{-\omega\left(\frac{\mu}{2}T_1 + \frac{\alpha\Lambda}{\sigma}\sin(\sigma T_1)\right)} \tag{31}$$

Because of $\Omega = \varepsilon\sigma$ and $u = u_0 + \varepsilon u_1 + \cdots$, we will obtain

$$u = c\cos(\omega t + \beta) + \frac{A}{\omega^2 - \Omega^2}\cos(\Omega t) + \mathcal{O}(\varepsilon) \tag{32}$$

The visualization for superharmonic resonant state is presented in Figure 9, which shows the oscillatory motion of a nonlinear spring when the frequency of the external force is zero. We can see in Figure 9a that the amplitude of the nonlinear spring motion fluctuates in a certain pattern.

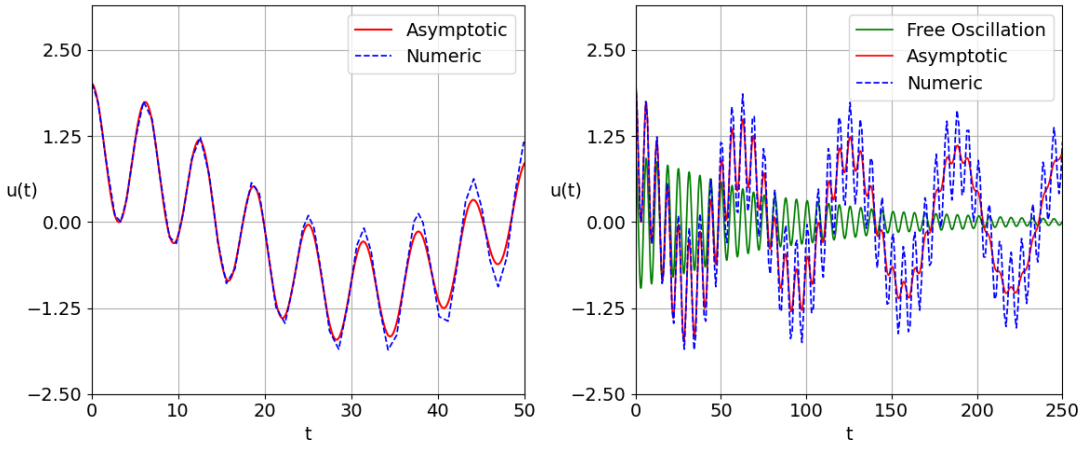

a. $t \in [0,50]$ b. $t \in [0,250]$

Figure 9. Visualization of a certain case where $\Omega = \varepsilon\sigma$ with $A = 1$, $\mu = 0.5$, $\omega = 1$, $\sigma = 10$, $k = 1$, and $\varepsilon = 0.01$.

The pattern referred to above can be seen clearly in Figure 9b. The chaotic behavior of the asymptotic solution is seen to decrease as time goes by, but remains non-smooth. The nonlinear spring continues to oscillate with a fairly large initial amplitude but slowly decreases, so that the motion of the system tends

to be oscillates around the equilibrium point. Further, the absolute error value for this scenario can be seen in Figure 10.

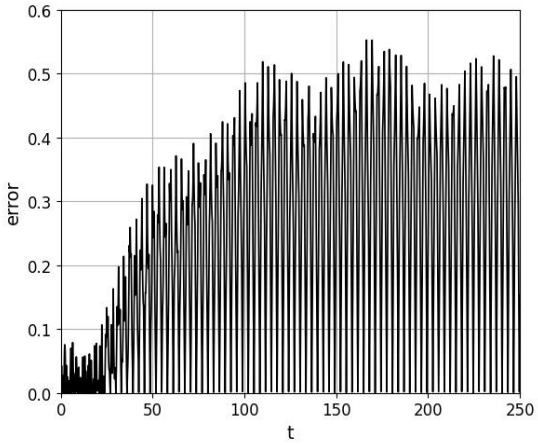

Figure 10. Absolute error of asymptotic and numerical solution for $\Omega \approx 0$.

Although the relative error produced is larger compared to other scenarios, the value is still relatively small. This is also consistent with the results shown in Figure 9a, which indicate that the difference between the asymptotic and numerical solutions becomes larger starting at $t \approx 25$. The absolute error also increases for $t > 50$, but it never exceeds 0.6. This occurs because the asymptotic and numerical solutions exhibit the same overall motion pattern, differing only in small oscillations that develop over time.

4. CONCLUSION AND SUGGESTIONS

This study shows that the nonlinear spring oscillation behavior under external force is greatly influenced by the relationship between the natural frequency and the external force frequency. In the primary resonance scenario, the oscillation amplitude increases due to resonance and then decays toward equilibrium. In the secondary resonance scenario, different cases such as nonresonant, superharmonic, subharmonic, and a special case produce different oscillation patterns, but overall, the amplitude tends to decrease over time. In addition, the solution curves produced by the numerical method are quite close to the solution results of the multiple time scale method, except for the special case where the excitation frequency is close to zero.

Future research could examine the model by linking it to practical applications and experimental validation for more robust results, as well as using other numerical methods for comparison. Then, a discussion regarding the dynamic analysis of each type of resonance that occurs in the model can also be carried out. In addition, the use of Lindstedt-Poincaré method on nonlinear spring models can also be considered as a variation of the asymptotic analytical method to observe the behavior of the model.

ACKNOWLEDGEMENT

The authors would like to thank LPPM Universitas Jenderal Soedirman for funding support through the Riset Dasar Unsoed (Batch II), Fiscal Year 2025, Grant No. 6.87/UN23.34/PT.01/V/2025.

REFERENCES

Binatari, N., van Horssen, W. T., Verstraten, P., Adi-Kusumo, F., and Aryati, L., *On the Multiple Time Scales Perturbation Method for the Differential-Delay Equations*, Nonlinear Dynamics, **112** (2024), 8431-8451, doi:10.1007/s11071-024-09485-z.

Chapra, S. C., and Canale, R. P. *Numerical Methods for Engineers*, Seventh Edition, New York: McGraw-Hill Education, 2015.

Dutta, T. K., and Prajapati, P. K., *The Dynamical Properties of the Duffing Equation*, International Journal of Engineering Research & Technology, **5** (2016), 500-503, doi:10.17577/IJERTV5IS120339.

Feng, G.-Q., *He's Frequency Formula to Fractal Undamped Duffing Equation*, Low Frequency Noise, Vibration and Active Control, **40** (2021), 1671-1676, doi:10.1177/1461348421992608.

Harjanto, E., van Horssen, W. T., and Tuwankotta, J. M., *On Resonances in A Weakly Nonlinear Microbeam Due To An Electric Actuation*, Nonlinear Dynamics, **104** (2021), 3157-3185, doi:10.1007/s11071-021-06495-z.

Holmes, M. H., *Introduction to Perturbation Methods*, Second Edition, New York: Springer, 2013.

Illahi, R. R., Marzuki, and Hudha, L. S., *Solution of the Duffing Equation Using Exponential Time Differencing Method*, Eigen Mathematics Journal, **7**(1) (2024), 16-18, doi:10.29303/emj.v7i1.195.

Kariarta, I. W., *Paradigma Materialisme Dialektis di Era Milenial*, Sanjiwani, **11** (2020), 71-81, doi:10.25078/sjf.v11i1.1534.

Kusumadjati, A., Hartati, S., Lutfin, N. A., Bidalo, F., Sari, S. D., Nurlina, and A, F., *Simulasi 1D Gerak Osilasi Terkopel di Sumbu Vertikal Untuk Menentukan Amplitudo Maksimum Benda Terbawah*. *Prosiding SNIPS 2017*, ITB Press, Bandung, 2017, 184-190.

Putra, G., Supmawati, M., and Prasetyo, B. *Method of Multiple Scales on Duffing Oscillator Equation and the Existence of Its Limit*. Transcendent Journal of Mathematics and Application, **2** (2023), 28-36.